Available online at www.sciencedirect.com
ScienceDirect
Engineering Failure Analysis 14 (2007) 765–782
ENGINEERING FAILURE ANALYSIS
www.elsevier.com/locate/engfailanal

Analysis of failures of guardrail base-plates in scissors crossovers of the Athens Metro: The role of foundation–structure interaction

Ioannis Anastasopoulos *, George Gazetas

School of Civil Engineering, National Technical University, Heroon Polytechneiou 9, Zografou, 13780 Athens, Greece

Received 30 June 2006; accepted 20 November 2006
Available online 16 January 2007

Abstract

Connecting parallel rail tracks, scissors crossovers typically consist of four turnouts and a central diamond crossing, while flange-way gaps provide wheel flange clearance at the points of rail intersection. Guardrails, supported through base-plates, provide wheel guidance in the area of the gap. In the Athens Metro, within less than a year in operation, fracturing of a vast number of guardrail support base-plates was reported. This paper documents the methodology and results of a comprehensive investigation of the possible causes of these failures. This premature cracking was initially investigated through stress and acceleration measurements. Subsequently, a three-dimensional finite element model was developed to analyse the dynamic behaviour of the system *with* and *without* foundation deficiencies. It was unveiled that only the model with foundation deficiencies could reproduce the measured response. The role of *foundation–structure interaction* (*FSI*) proved doubly detrimental for the performance of the system: (i) the initial defective curved shape of the sleepers induced large bending pre-stress on the base-plates, and (ii) the defective gap-dominated foundation increased the flexibility of the system leading to further excessive sleeper bending, and thereby to increased distress of the base-plates. The combination of the two deficiencies was deemed responsible for the observed failure. The method of installation was shown to be of critical importance for the durability of the crossover.

Keywords: Railway engineering; Turnouts; Scissors crossovers; Base-plate failure; Finite element analysis

1. Introduction

Turnouts are used to allow two railway tracks to intersect at the same level. As depicted in Fig. 1a, a standard turnout consists of three parts: (a) the switch blades – movable parts controlling the direction of train passage, (b) the crossing – the central part of the turnout where the rails intersect, and (c) the closure rail – the part of the turnout between the switch blades and the crossing. At the point of rail intersection (heart)

* Corresponding author. Tel.: +30 2107723383; fax: +30 2107722405.
E-mail address: ianast@ekpe.gr (I. Anastasopoulos).

1350-6307/$ - see front matter © 2006 Elsevier Ltd. All rights reserved.
doi:10.1016/j.engfailanal.2006.11.004

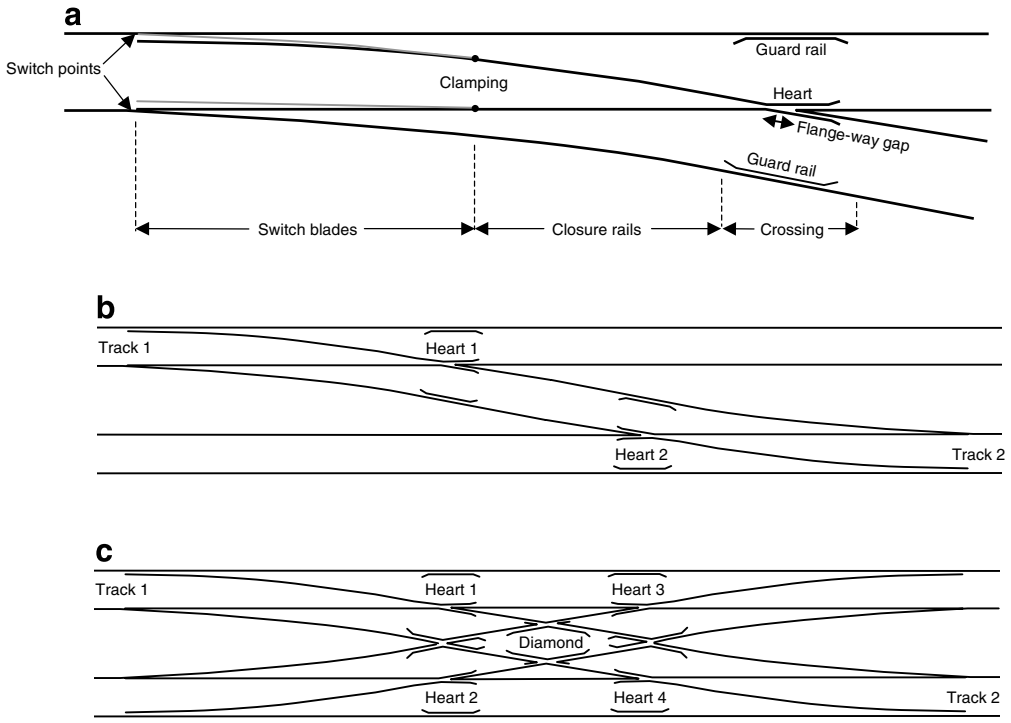

Fig. 1. (a) Single turnout and its main components, (b) combination of two turnouts to form a *crossover*, and (c) combination of four turnouts with a central diamond crossover to form a *scissors crossover*.

a gap is necessary to provide wheel flange clearance. Due to this gap, termed flange-way gap, the wheel is temporarily unguided. Guardrails are installed to provide the necessary (horizontal) wheel guidance [1]. The guardrails are supported through special metal plates, the guardrail support base-plates. A detailed discussion on turnout geometry and design aspects can be found in [2]. Two parallel rail tracks can be connected with two turnouts to allow traffic from one track to the other. Such a combination is termed *crossover* (Fig. 1b). Two parallel tracks can also be connected with a set of four turnouts combined with a central diamond crossing, termed *scissors crossover* (Fig. 1c).

Twenty-six scissors crossovers manufactured by *LAEIS-Weichenbau* were installed in the Athens Metro (Fig. 2). Just a year after opening to traffic (January 2000), fracturing of several guardrail support base-plates (Fig. 3) was reported. The premature cracking was first investigated through stress measurements [3]. After analyzing the results of the measurements, the track-work group (*SPIE Batignolles S.A.*) and the manufacturer of the crossovers (*LAEIS-Weichenbau*) decided to slightly modify the design of the base-plates, by increasing the thickness of the base flange of the plates from 15 to 20 mm. New measurements [4] after installation of the modified base-plates showed significant stress reduction. However, cracking of the base-plates persisted.

A new set of (mainly vertical) acceleration measurements [5] compared a brand-new turnout, X16, and a turnout under traffic, X20. The data was utilised to capture the vibration modes of the two turnouts. It was concluded that the cause of failure was the defective ‘‘suspension’’ of the sleepers, which led after a short time (under traffic) to significant stiffness reduction of the system. It was recommended that the whole design of the foundation be reviewed.

This paper documents the methodology and results of a subsequent study aimed at unveiling the causes of failure [6]. Emphasis is given on the role of *foundation–structure interaction* (*FSI*). *Structure* refers to everything that lies above the sleepers: rails, guardrails, and base-plates. *Foundation* refers to the sleepers and their ‘‘suspension’’. It will be shown that the role of *FSI* is double and detrimental for the behaviour of the system.

First, we conduct a comprehensive review of the recorded data, for exploiting the results and developing an understanding of the mechanisms contributing to failure. A three-dimensional non-linear finite element (FE)

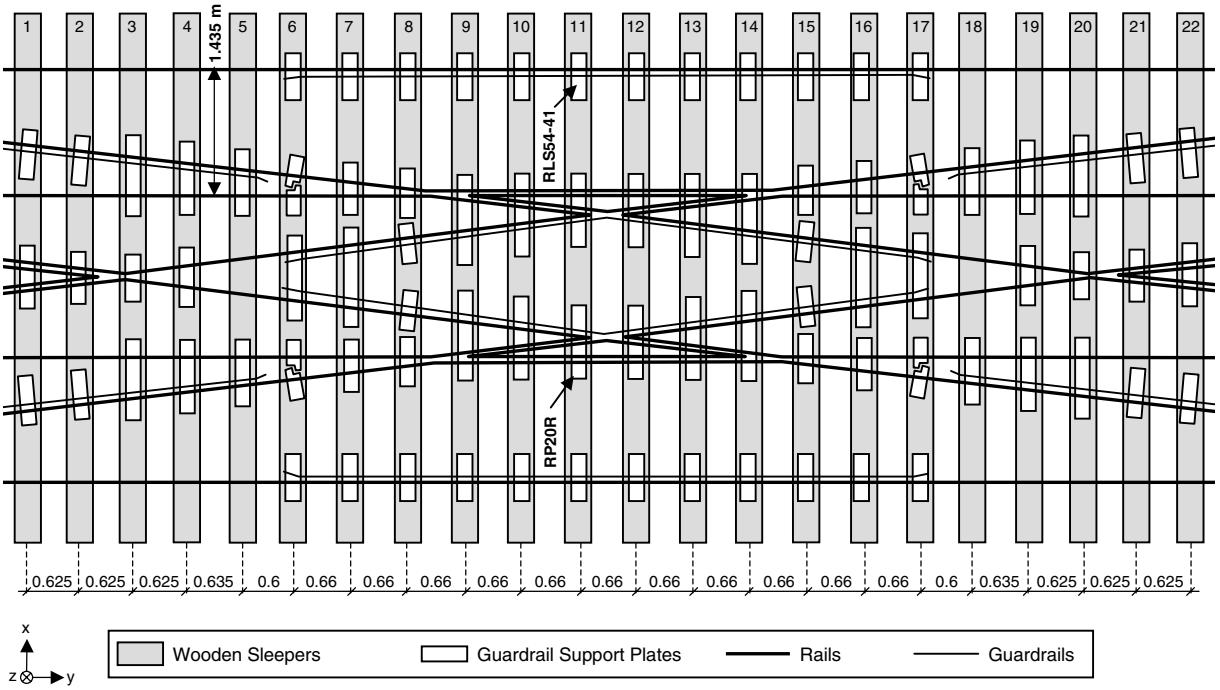

Fig. 2. Plan of the scissors crossover installed in the Athens Metro.

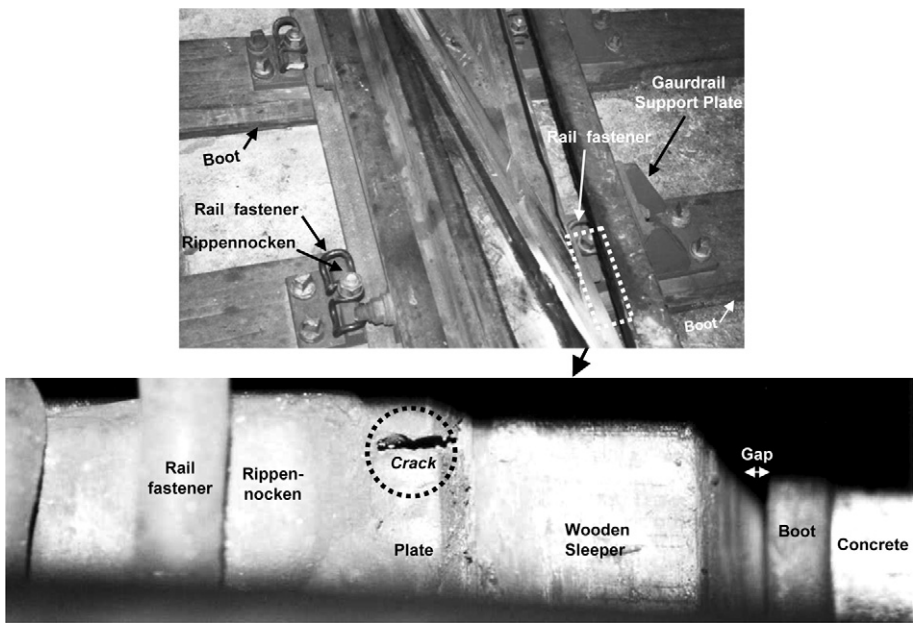

Fig. 3. Initiation of a crack in a guardrail support plate near the area of crossing. Notice the gap between the wooden sleeper and the rubber boot.

model is then developed to analyse the dynamic response of the system with and without foundation deficiencies. Finally, the effectiveness of possible corrective measures is explored, concluding with the final solution to the problem.

2. Force and strain measurements – June 2001

The first force and strain measurements were conducted in June 2001 by *TRCpro* [3]. As depicted in Fig. 4, force transducers and strain gages were installed on crossover X20, situated between Panormou and Katechaki stations on Line 3 [7]. The strain gages were installed at the area of observed fracturing on two different plates: (i) RLS54-41 (Fig. 5a), and (ii) RP20R (Fig. 5b), with the latter significantly longer.

After installation of the measuring equipment, the plates were mounted back on the sleepers. During the fastening process non-negligible initial stresses σ_{xx} were recorded. As shown in Fig. 6, these stresses on plate RLS54-41 ranged from −80 MPa to −135 MPa (compressive) at the bottom of the base flange, and from 75 to 240 MPa (tensile) on top of the base flange; on plate PR20R they were lower, not exceeding 70 MPa. *TRCpro* attributed this difference to the higher flexibility of plate RP20R compared to RLS54-41.

However, during installation σ_{xx} reached 180 MPa on RP20R. Then, by adjusting the plate bolts while monitoring σ_{xx}, minimisation of stresses was achieved. The procedure took more than 45 min (2800 s). The same procedure was attempted for plate RLS54-41 but not with the same success, although the adjusting took more than 1 h (4000 s). In practice, the plates are installed un-instrumented; obviously such a monitored-stress adjustment installation procedure could not have been applied.

A plausible explanation of the cause leading to these initial stresses is illustrated in Fig. 7. In the ideal case of a perfectly straight sleeper, the fastening process should not produce any stress (Fig. 7a). However, if the sleeper is not straight, when the base-plate is installed and screwed on it, it is forced to bend and follow the curved shape of the sleeper (Fig. 7b). In our terminology, this is the first role of *FSI*. Utilising the 3-D FE model discussed in the sequel, we conclude that a curvature equivalent to 5 mm height difference from the beginning to the end of plate RP20R (i.e. ∼0.7% inclination = 5 mm/870 mm) is enough to produce tensile stresses (due to bending) of about 210 MPa on top of the base flange. Naturally, not all sleepers are equally curved. In addition to their initial non-perfect shape, the actual curvature depends on a number of factors such as humidity and weathering. Each sleeper is a separate case and only through several measurements could the curvature be reliably inferred.

The *TRCpro* measurements were performed on two plates only. Hence, given the available data we can only assume that the initial stresses can be at least as high as 250 MPa (tensile) at the top of the base flange and at

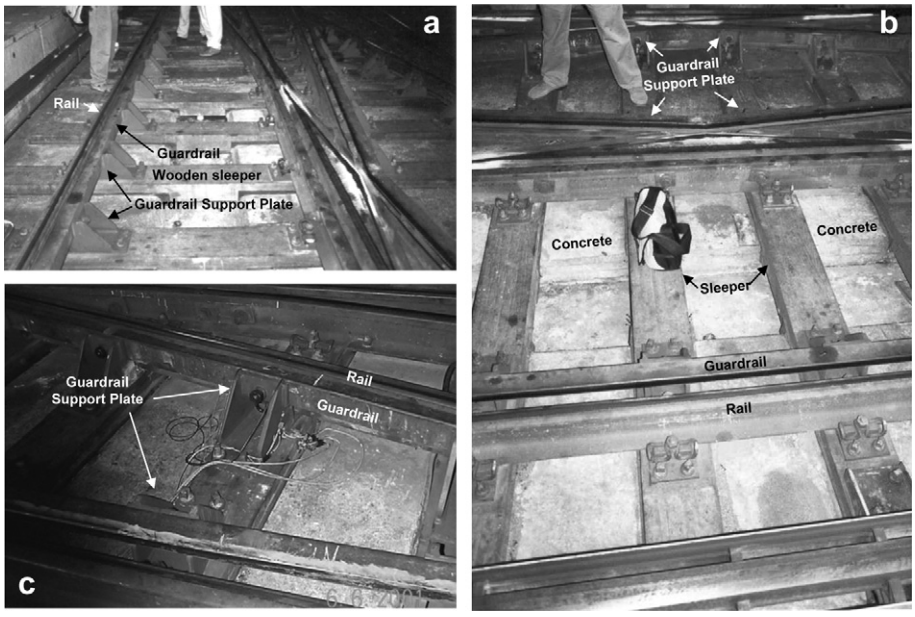

Fig. 4. (a) General view of the scissors crossover, (b) zooming in the diamond, and (c) guardrail support base-plate assemblies with installed measuring instruments [2].

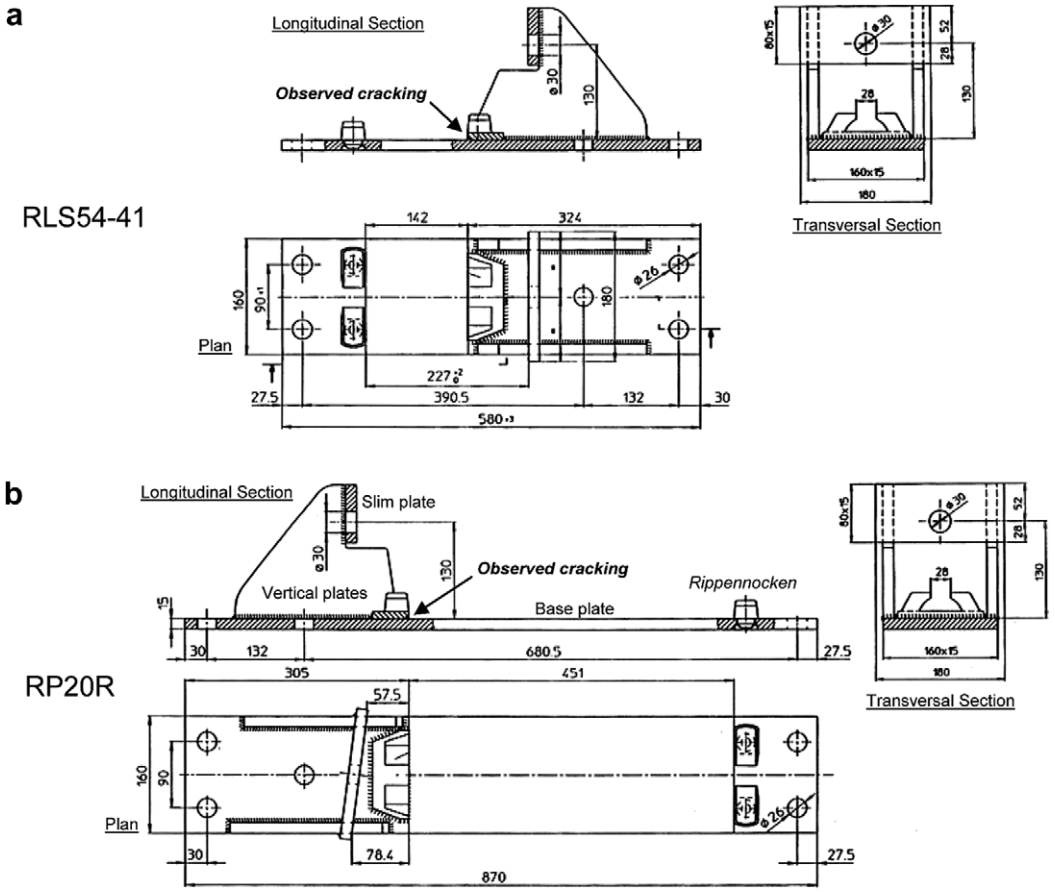

Fig. 5. Plan and cross-sections of base-plate assemblies: (a) RLS54-41, and (b) RP20R.

least as low as −135 MPa (compressive) at the bottom. The possibility of higher initial stresses (due to larger sleeper curvature) cannot be excluded. The curvature of the wooden sleepers may increase with time due to environmental factors such as changes in humidity and temperature. This may explain why there was no problem at the very beginning.

A typical stress time history (top of base flange, plate RP20R) during train passage (80 km/h, in straight direction) is depicted in Fig. 8. Each train (manufactured by SIEMENS) consists of six cars. In the same figure we focus on a time window comprising the first bogie of the first car. Then, we focus further on a smaller time window that comprises only one wheel (the second of the first bogie). First a positive stress pulse takes place; then a negative. The former lasts for about 5 ms while the latter for about 6 ms. In this particular case, σ_{xx} reaches 115 MPa and −170 MPa, respectively.

The same procedure was applied to all wheels and to all sets of measurements. The observed stress pattern and pulse duration was qualitatively the same in all cases. These dynamic stresses are due to wheel *impact* on the rail at the area of crossing, which is the result of the existence of the flange-way gap, taking place even when the train is passing the crossover at a straight.

According to *TRCpro* [3] every shock exerts a damped oscillation of frequency $f \approx 30$ Hz, for 3–5 cycles. Naturally, not all of these cycles are equally detrimental for fatigue. *TRCpro* also concluded that the quasi-static loading due to train passage does not cause significant stressing. This is directly observable in the measurements. Most crossovers are passed (at a straight) by 20 trains per hour (one train per 3 min) during peak traffic hours, but are only rarely crossed. Therefore, it can be inferred that train straight passing (not crossing) is the most critical factor for fatigue failure.

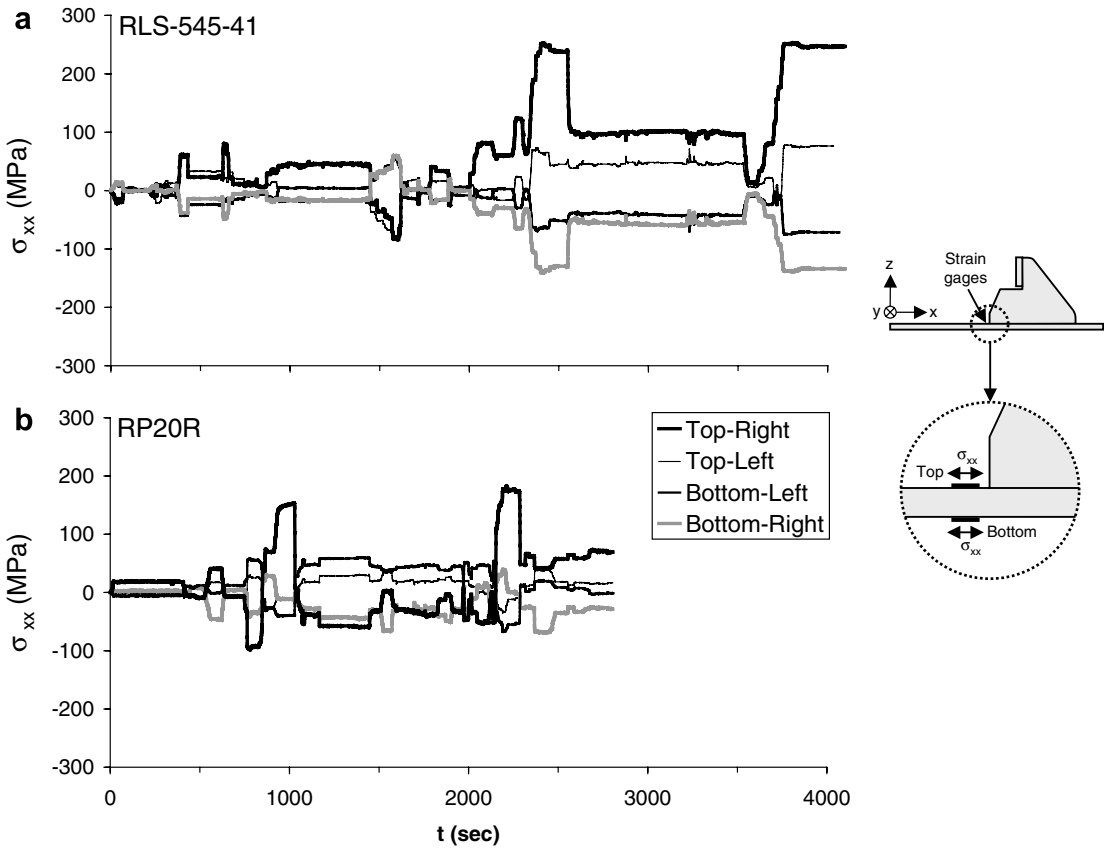

Fig. 6. Initial stresses measured in the guardrail support plates [2]: (a) RLS-545-41, and (b) RP-20R.

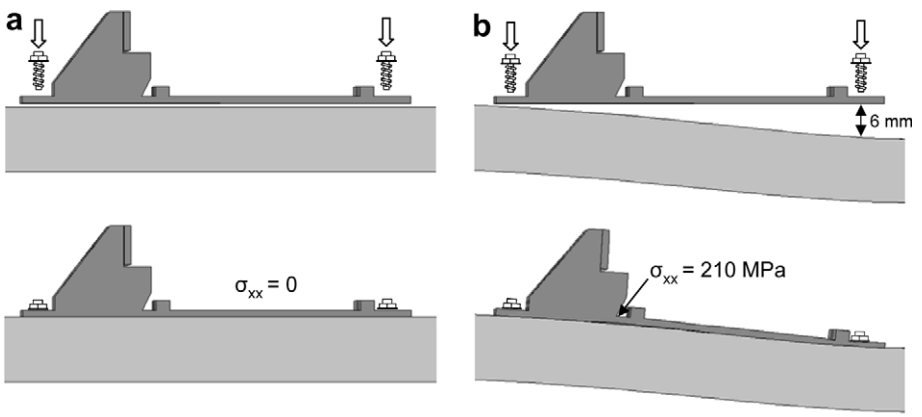

Fig. 7. Fastening of the guardrail support plate on the sleeper: (a) "ideally" straight sleeper; (b) "defective" curved sleeper. In the latter case, the fastening will unavoidably cause initial bending of the base-plate (tensile stress at the top and compressive at the bottom of the flange).

3. Force, strain, and displacement measurements – September 2001

A new measurement campaign [4] was conducted after implementing the following modifications:

(i) the thickness of the base-plate was increased from 15 mm to 20 mm,
(ii) the moment of inertia of the guardrail was reduced by 90%,

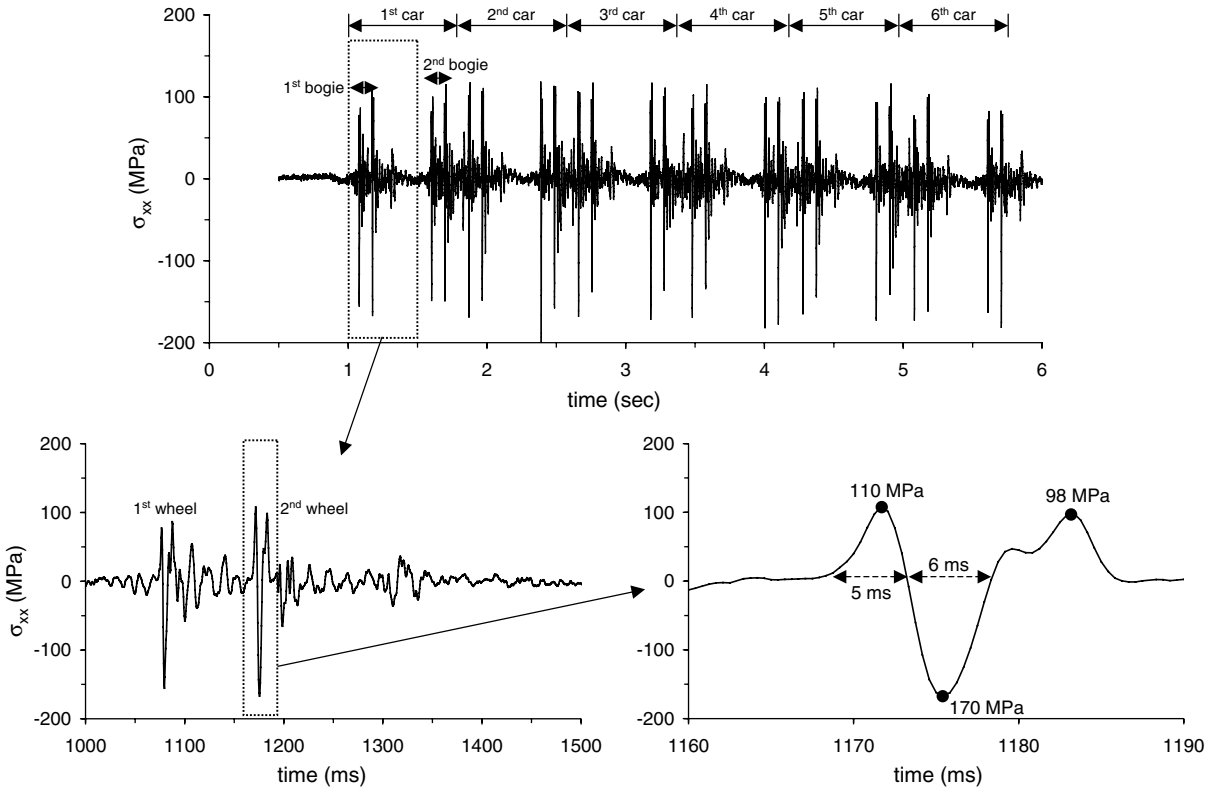

Fig. 8. Measurement of longitudinal stress σ_{xx} (top of base flange, RP20R) during train passage [2]. Top: complete time series; bottom: focusing on σ_{xx} during a single wheel passage.

(iii) the rail fixing cam (“Rippennocken”) was replaced with rolled cams,
(iv) a new fixing screw between the sleeper and the plate near the critical area was installed to reduce plate deflection, and
(v) the size of the mounting holes between slim-plate and guardrail was increased to reduce pre-stressing during mounting caused by geometrical inaccuracies.

The new measurements showed significant stress reduction, ranging from 60% to 90%. The reduction was smaller in plates nearest to the flange-way gap. This was attributed [4] to a reduction of the guardrail stiffness.

Vertical displacements during train passage were now also measured. The rail displacement was between 3.0 and 3.5 mm. With such small displacement the problem should have ceased. Unfortunately, although fracturing did not occur as often as before, the problem persisted. Such a behaviour might appear as a paradox; it could be explained by recourse to the first role of *FSI*.

For the manufacturing of the new plates steel quality St42 was used, instead of St52 of the older plates. This reduction in steel strength (of the order of 20%) should not have been a problem since it was overshadowed by the dynamic stress reduction (measured in the order of 60–90%). However, as already discussed, the plates also suffer from initial stresses due to sleeper curvature (the first role of *FSI*). These stresses could not be significantly reduced: the sleepers remained exactly the same. In fact, the increase of the thickness of the bottom plate (from 15 to 20 mm), and hence of the stiffness of the whole plate, would tend to cause the opposite effect.

The initial stresses, σ_m, have a pronounced effect on the critical fatigue strength, σ_k, of the steel. As depicted in Fig. 9, if σ_m were equal to zero, σ_k for St52 would equal 250 MPa, and for St42: $\sigma_k = 190$ MPa [8]. However, taking *FSI* into account we observe that for σ_m ranging from 250 MPa to 150 MPa, σ_k ranges from 110 MPa

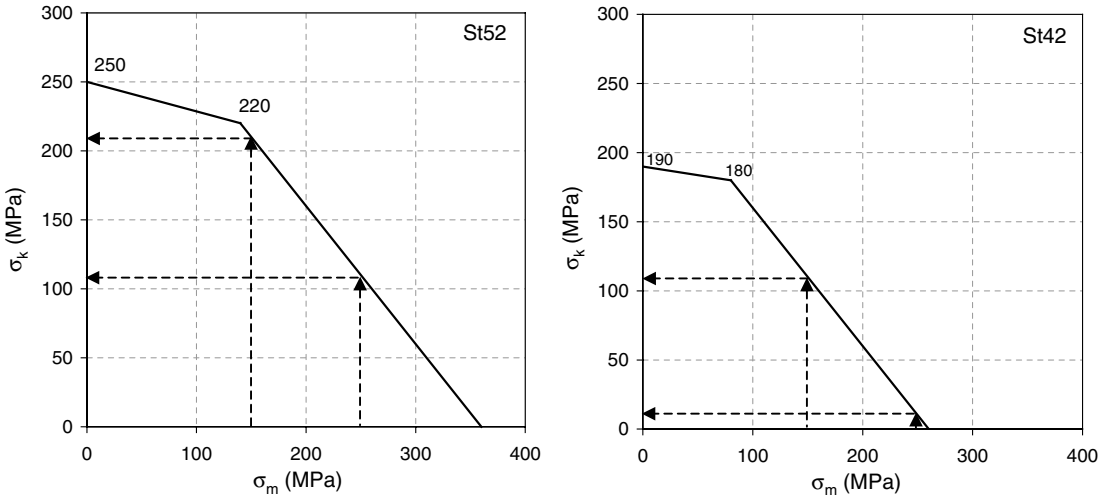

Fig. 9. Critical fatigue stress σ_k as a function of the initial stress σ_m for St52 and St42 [7].

to 200 MPa for St52. In the case of St42 (used in the modified design), for $\sigma_m = 250$–150 MPa the fatigue strength σ_k ranges from 20 MPa to 110 MPa. Thus, due to the un-intended initial distress of the plates (first effect of *FSI*), the St42 plates had reduced strength reserves to escape fatigue failure.

4. Acceleration measurements and failure modes analysis – May 2002

Having concluded that the aforementioned modifications did not exactly have the desired effect, a new set of measurements was conducted [5]. Vertical acceleration measurements were conducted on a brand-new crossover (X16), and on an already "damaged" crossover under traffic (X20). The measurements were analysed to capture the vibration modes of the two turnouts. Two different methods were applied: (a) an impact-controlled hammer was used to produce shock excitation (modal test), and (b) passing trains were used as the excitation. The mode shapes of the two methods were found to differ only slightly. As depicted in Fig. 10, the modal test on the new crossover X16 revealed a dominant response frequency at 54 Hz and a secondary one at 76 Hz. The first mode was nearly *symmetric*, while the 76 Hz mode *anti-symmetric*. The behaviour of crossover X20, which had been under traffic ever since Line 3 went into operation (January 2000), was different: a 35 Hz dominant response frequency was observed, accompanied by other modes at 47–55 Hz, and some secondary ones at 63 Hz and 74 Hz. The dominant mode was not symmetric.

It became evident that the older crossover (X20) was less stiff than the new one (X16): its dominant frequency was at 35 Hz, instead of 54 Hz. Furthermore, the dominant mode of X20 was not symmetric, implying the existence of non-symmetric defects. Assuming that both crossovers were constructed with the same method, and that X20 at the start of its life responded the same as X16, it can be concluded that the system becomes more flexible with time in service. According to [5], this deterioration with time could be attributed to the following: due to bending of the sleeper the concrete became more and more damaged, and as a consequence, the rectangular boot print became trapezoidal, making the rotation of sleepers easier and thereby the whole system more flexible. This resulted in reduction of the fundamental frequency, while at the same time damping was reduced and the amplitude of the motion increased. The damage procedure was supposed to initiate from the defective *suspension* (i.e. the support) of the system, attributed to the excessive softness of the installed micro-cellular pad (underneath the sleeper), as well as to the fastening procedure of the rubber boot. As it will be shown in the sequel, this is the second effect of *FSI*.

The existence of a 5–8 mm "play" (i.e. gap) between the sleepers and the concrete was already pointed out. Pieces of the micro-cellular pad were reported to have been ejected. The reason for this type of damage was attributed to the fastening method. As schematically illustrated in Fig. 11, according to the specifications of COGIFER [5] the micro-cellular pad–rubber boot assembly should have been nailed to the

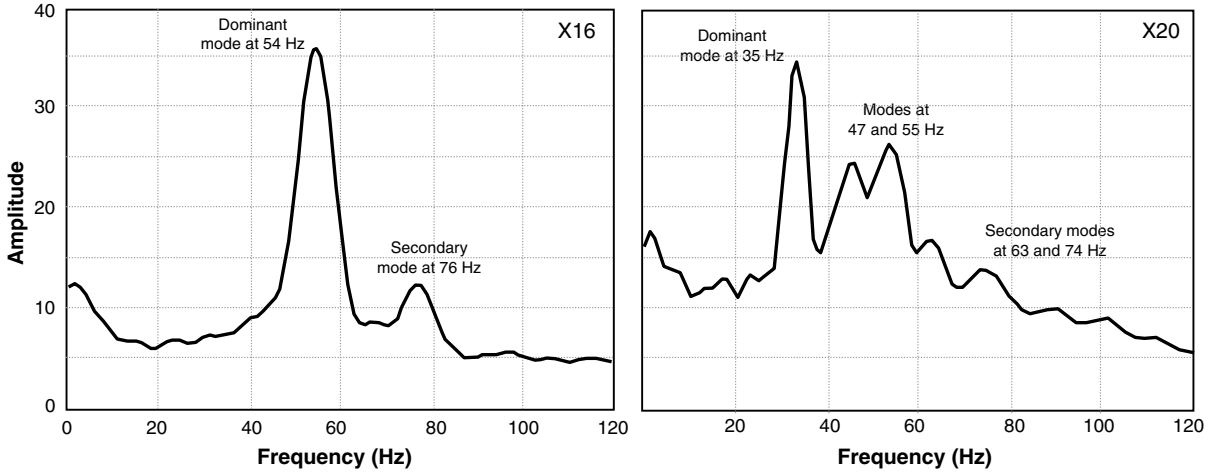

Fig. 10. Recorded response spectra in a newly built turnout (X16) compared to an identical turnout already in service (X20) [4]. The older turnout (X20) has clearly become more flexible.

sleepers at distances not exceeding 30 cm. Nailing should have been used in the bottom of the sleepers and on both sides. If the nails were placed at larger distances (improper installation), contact between sleeper and pad/boot would be less rigorous. Contact between sleeper, micro-cellular pad, and rubber boot should be attained at three points every 30 cm. If instead of the three nails, ties were utilised (as suspected), then the fixing points would be only two (at the two edges). Given that the rubber boot–pad–sleeper assembly was used as the casing for the concrete sub-base, any loss of contact between them would result in an imperfect concrete surface, with small gaps between concrete and sleeper, in accord with the observations of [5].

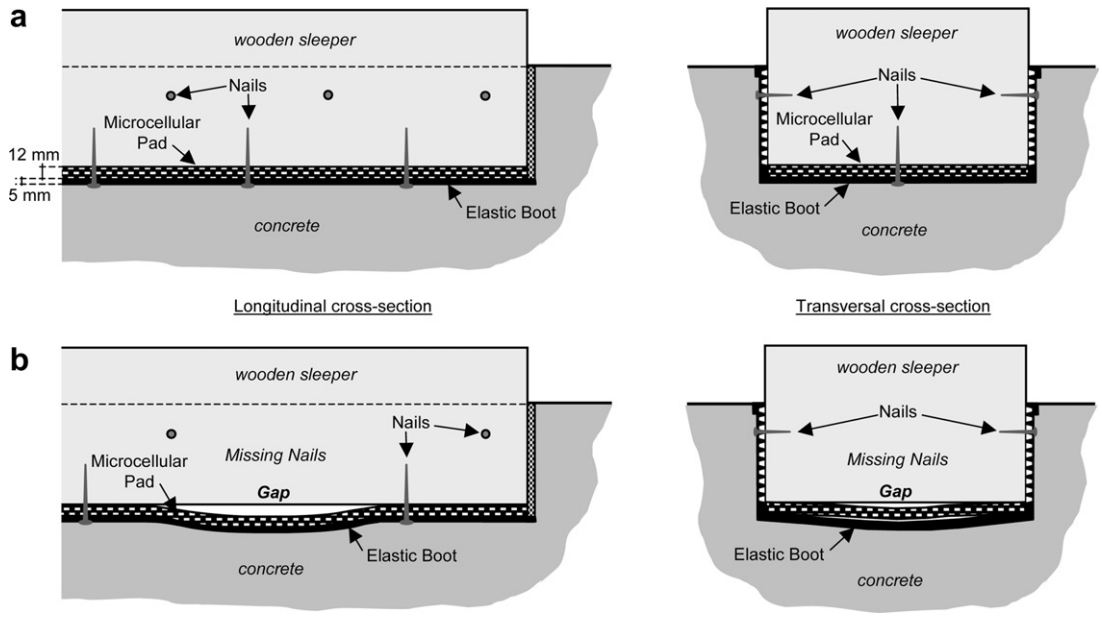

Fig. 11. Foundation of the turnout: (a) proper installation according to the specifications [4], and (b) improper installation. Since the sleeper with the micro-cellular pad and the rubber boot is used as the casing for the concrete sub-base, the quality of the foundation relies on proper nailing. With sparse nailing, gaps may be generated between the concrete and the rubber boot.

5. Site visit observations: the role of gaps and imperfections

Before proceeding with the analysis, we shortly discuss the findings of our site visit. We visited the crossover before the Station of ''Daphne'', along Line 2 [7]. As shown in Fig. 12a, near the edges of the sleepers we observed signs of concrete spalling, which was quite systematic; it was attributed to excessive vibration due to the presence of gaps at the concrete–boot–pad–sleeper interface. Fig. 12b illustrates a rather common case of an ejected pad, implying the existence of gaps. Our findings compare well with [5] (which refers to a different crossover), proving that the problem is not site-specific. Signs of damage seem to be present in the concrete as well as some gaps and imperfections at the contact interface between sleeper, micro-cellular pad, and rubber boot. However, we did not observe huge gaps and ''plays'' (of the order of 5–8 mm). Although it was impossible to measure every single gap, our feeling was that gaps were of the order of 1–3 mm at most. An exception is the area near the gutter where some pads had been ejected. The ''play'' in such locations could be much higher.

The installed micro-cellular pad is undoubtedly an extremely soft material: its static stiffness K_{st} ranges from 1300 to 2000 kN/m while its dynamic stiffness K_{dyn} is higher, ranging from 2300 to 3700 kN/m. We note for comparison that the static and dynamic stiffness of the railpad (installed between the base-plate and the rail) is 100 and 300 MN/m, respectively – two modes of magnitude higher. Since the micro-cellular pad is made of rubber it is nearly an incompressible material, implying a Poisson's ratio $v = 0.49$. A vertical force F applied on the pad will produce vertical stress σ_z and deformation ε_z. Being incompressible ($v = 0.49$), the pad will tend to expand in the lateral direction:

$$\varepsilon_x = \varepsilon_y \approx \varepsilon_z/2 \tag{1}$$

As schematically illustrated in Fig. 12c, if the micro-cellular pad is free to expand, ε_z will only depend on the material stiffness, or equivalently its Young's modulus E. On the other hand, if the pad is laterally constrained, due to its incompressibility it will behave as an infinitely stiff material.

A simple analogy can be drawn between the behaviour of rubber and water. It is well known that water is also incompressible, but its shear stiffness is zero. If water is poured inside a water-tight cylinder, then the piston cannot easily be pressed down: being incompressible, water responds in an extremely ''stiff'' manner. If we

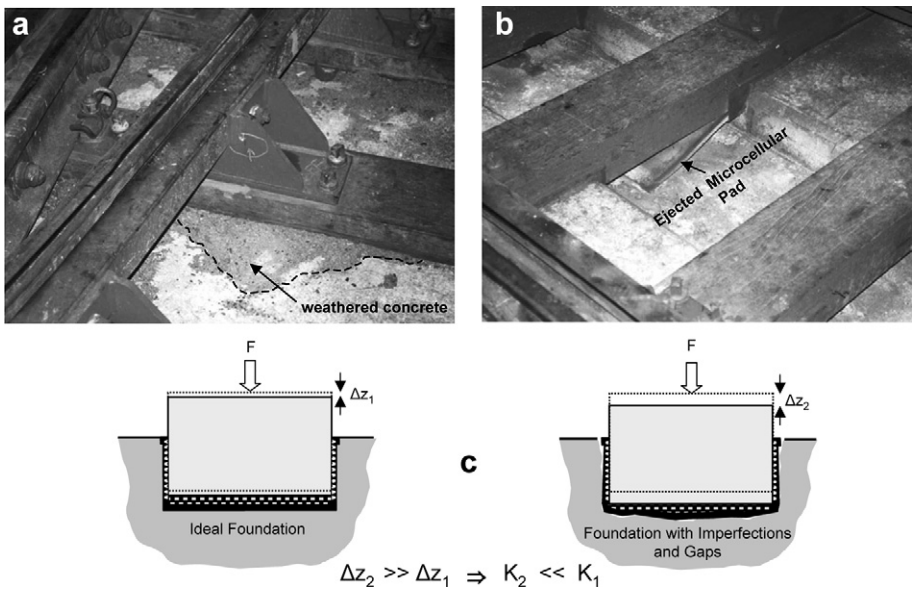

Fig. 12. (a) Signs of concrete weathering, (b) ejected micro-cellular pad: clear indication of the existence of gaps at the foundation, (c) illustration of stiffness reduction due to presence of gaps.

make an opening to the cylinder (so that water can drain), the piston will be much easier to press: the ''stiffness'' of the system will be reduced significantly, depending on the size of the opening and the speed of loading. The same principle applies to the micro-cellular pad. If it is fully and perfectly embedded inside the concrete (confined compression), it behaves in an extremely ''stiff'' manner responding with an *effective stiffness* much larger than its material stiffness. However, in light of the existence of (lateral) gaps the pad is allowed to expand, and the *effective stiffness* becomes equal to the material stiffness. Being unaware of the exact size and number of potential gaps, in the consequent 3-D FE analysis we treat them through reduction of the *effective Poisson's ratio* ν' of the material. Thus, $\nu' = 0.49$ implies perfect embedment, while $\nu' = 0.40$–0.30 implies existence of (lateral) gaps of increasing importance.

6. 3-D Finite element modeling methodology

In the previous sections we reviewed the results of three different measurement studies [3–5], to shed light to the causes of failure of the base-plates. *FSI* is believed to have played a double detrimental role: (i) the initial defective curved shape of the sleepers induced large bending pre-stress on the base-plate, and (ii) due to the defective gap-dominated ''suspension'' of the sleepers, the system became too flexible. The latter is believed to have amplified the dynamic response of the system subjected to wheel impact in the area of the flange-way gap. In this section we develop a three-dimensional finite element (FE) model to analyse the response of the *foundation–structure* system.

Analyses are conducted utilising the code ABAQUS [9]. We isolate and analyse sleeper No. 11 (see Fig. 2) which is the closest to the flange-way gap (the source of dynamic distress). As depicted in Fig. 13, we analyse the whole system consisting of (from bottom to top): rubber boot, micro-cellular pad, sleeper, guardrail support base-plates, rail pads, rails, and guardrails. We analyse the initial base-plate design with base flange thickness of 15 mm. The effect of gaps at the sleeper–micro-cellular pad–rubber boot–concrete interface, i.e. the second effect of *FSI*, is investigated parametrically through application of the previously discussed concept of *equivalent Poisson's ratio* ν'. Springs are placed at the lateral boundaries of the FE model to model the interaction with neighboring sleepers. The FE model without boundary springs is first analysed to derive the vertical and lateral stiffness of the isolated sleeper. The derived stiffnesses are utilised to calibrate the boundary interaction springs.

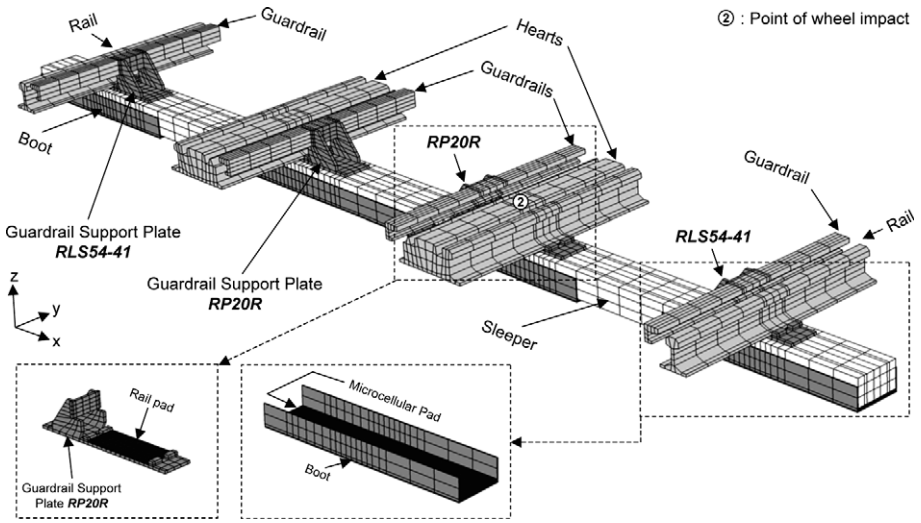

Fig. 13. Three-dimensional finite element discretisation. We isolate and analyse the sleeper that is closest to the flange-way gap (No. 11, see Fig. 2).

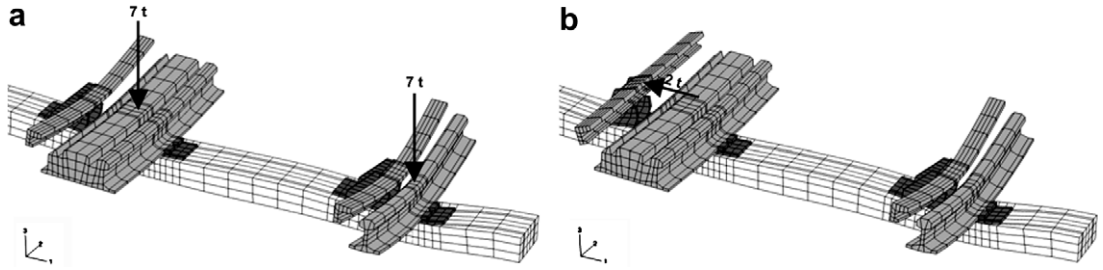

Fig. 14. Pseudo-static analysis – deformed finite element mesh: (a) vertical loading of 14 t due to wheel travel (one axle), (b) lateral force of 2 t due to wheel impact on the guardrail.

7. Quasi-static analysis

All of the measurement studies [3–5] agree that the main source of distress of the crossover is the dynamic impact-induced vibration, and not quasi-static loading due to wheel-set traveling over the rails. To verify this, before proceeding to the dynamic analysis of the system, we conduct a quasi-static analysis of wheel travel. As depicted in Fig. 14a, we apply a vertical load of 14 t representing the weight on one axle of a metro vehicle. As already discussed, during passage over the flange-way gap the wheel is temporarily laterally unsupported, and guidance is achieved through the guardrail. The lateral loading on the guardrail was measured [3] to range between 0.5 t and 2 t. So, in addition to wheel travel, we also load our FE model with a quasi-static lateral force of 2 t on the guardrail (Fig. 14b). The effect of gaps and imperfections, i.e. the second role of *FSI*, was also investigated utilising the *effective Poisson's ratio* concept discussed previously.

Several quasi-static analyses were performed to parametrically investigate the effect of the stiffness of the rail pads (k_{railpad}) and the micro-cellular pad ($k_{\text{micr-pad}}$), in addition to foundation gaps and imperfections (v'). In all cases, vertical displacements Δz were practically negligible. Even in the worst case scenario ($k_{\text{railpad}} = 100$ MN/m, $k_{\text{micr-pad}} = 1300$ kN/m, and $v' = 0.30$) Δz did not exceed 0.6 mm (compared to 3 mm of the measurements). More importantly (Fig. 14a), since the loading is applied on both rails the sleeper moves downwards as a whole, without excessive bending. Consequently, the stress in the area of failure does not exceed $\sigma_{xx} = 40$ MPa even in the extreme case of 2 t lateral loading (Fig. 14b). Such stress magnitudes could not possibly have led to the observed premature fatigue failure of the base-plates (see Fig. 9). [In contrast (as it will be shown in the sequel), when the system is subjected to impact-induced excitation, the dynamic loading is applied on one rail only (the one with the flange-way gap) causing significant sleeper bending.]

8. Eigen-frequency analysis

The dynamic response of the system is first approached through eigen-frequency analysis. The main aim is to extract the dominant vibration mode shapes of the system along with the dominant natural frequencies. As for the quasi-static analysis, the second effect of *FSI*, i.e. the effect of gaps and imperfections, was investigated through the *effective Poisson's ratio* v'. The latter was varied parametrically, from $v' = 0.49$ to 0.30. The first ($v' = 0.49$) represents an ideal foundation, where sleeper, pad, boot, and concrete are in full contact; while the latter ($v' = 0.30$) refers to defective foundation with gaps and imperfections. Before proceeding with the results, it must be noted that this type of analysis can only be elastic. This means that the effect of de-bonding and separation–uplifting that may occur between different components of the system cannot be incorporated in the model. In other words, it is unavoidably assumed that the micro-cellular pad can transfer tension from the sleeper to the rubber boot, and the latter can transfer this tension to the concrete sub-base. This is obviously an unrealistic simplification, as these components are not tied together to be capable of transferring tension from one to the other.

Fig. 15a depicts the first two mode shapes for the case of the ideal system ($v' = 0.49$). The corresponding natural frequencies are $f_1 = 91$ Hz and $f_2 = 92$ Hz, respectively. The first mode is anti-symmetric, and the second symmetric. Observe that in the first mode the guardrail tends to move away from the rail, while in the

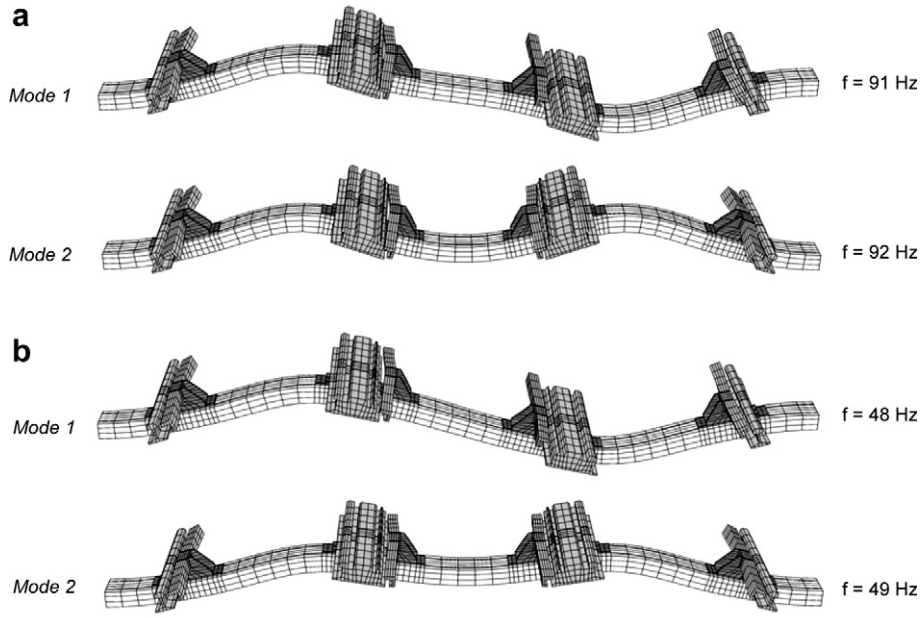

Fig. 15. Dynamic eigen-value analysis – deformed finite element mesh for the first two eigen modes: (a) ideal foundation ($v' = 0.49$), (b) defective foundation with gaps ($v' = 0.30$).

Table 1
Eigen-frequency analysis (Hz): the effect of foundation gaps – the 2nd role of *FSI*, expressed through the *effective Poisson ratio* v', on the eigen frequencies of the system

	Ideal system $v' = 0.49$	"Some" gaps $v' = 0.40$	"More" gaps $v' = 0.35$	"Many" gaps $v' = 0.30$	$v' = 0.30$ and *ejected railpad*
Mode 1	91	55	51	48	45
Mode 2	92	56	52	49	46

second towards the rail. Accordingly, Fig. 15b illustrates the first two mode shapes assuming defective foundation with "many" gaps and imperfections ($v' = 0.30$). While the mode shapes remain practically the same, the natural frequencies of the system are reduced significantly to 48 Hz and 49 Hz. Table 1 summarizes the effect of foundation gaps (the second *FSI* effect) on reducing the natural frequencies of the system. Interestingly, the reduction is not linear: while reducing v' from 0.49 to 0.40 reduces f_1 form 91 Hz to 55 Hz, further reduction of v' to 0.30 reduces f_1 marginally to 48 Hz. Even if we assume that the railpads near the gutter have been ejected (as observed, see Fig. 12b) f_1 does not become much less than 45 Hz.

The second *FSI* effect starts becoming evident: foundation gaps and imperfections clearly increase the flexibility of the system, leading to increased bending of the sleepers. Our results are in qualitative agreement with the measured system response [5]. As already discussed, the older crossover X20 was found to be less stiff than the brand-new X16: $f_1 = 35$ Hz instead of 54 Hz. Quantitatively, the comparison is not excellent. Even with $v' = 0.30$ and with ejected pads, our analysis yields $f_1 = 45$ Hz instead of the measured 35 Hz. A plausible explanation for this discrepancy: the effect of de-bonding and separation between different system components, which could not have been incorporated in this type of analysis; however, it will be taken into account in the dynamic wheel impact analysis discussed in the sequel.

9. The source of dynamic distress: wheel impact

As already discussed, at the point of rail intersection the flange-way gap is necessary to provide wheel flange clearance. It will be shown that this discontinuity is the main source of dynamic distress of the crossover. As

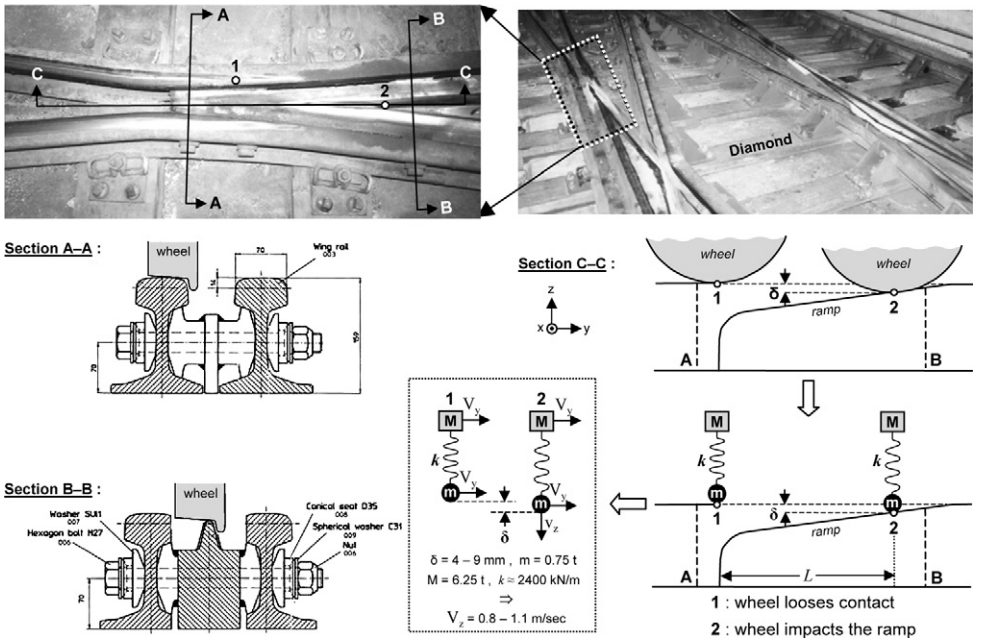

Fig. 16. The main source of dynamic distress of the turnout: the flange-way gap. When the wheel (of mass m) passes over this gap it first looses contact at point "1", then follows an accelerating movement due to the compressed (by the weight of the car Mg) suspension spring (k), and eventually impacts the ramp at point "2". The vertical impact velocity V_z depends on the geometry of the ramp (gap δ, length L), the properties of the metro car (m, M, and k), and the horizontal train passage velocity V_V.

depicted in Fig. 16, the wheel (of mass m) approaches the flange-way gap with speed V_y. Reaching point "1" (see section A–A) it looses contact with the supporting rail. In the horizontal sense (y) it continues its travel with the same speed. In the vertical sense (z) the wheel "falls", following an accelerated movement. However, it is not *free falling* with the acceleration of gravity. This could only happen if it were rigidly connected to the rest of the car.

In reality, the wheel "falls" with greater than the gravitational acceleration. This is due to the primary suspension of the vehicle. A typical train car comprises three main components: the car body, the bogie, and the wheel-set (also termed "non-suspended mass"). The car body rests on the bogie through the secondary suspension, and the wheel-sets are suspended from the bogie through the primary suspension. Track irregularities are mainly "felt" by the primary suspension [2]. Due to the weight of the car body (Mg) corresponding to one wheel, the primary suspension spring (one per wheel) is initially compressed (before reaching point "1"):

$$z_{\text{ini}} = Mg/k \tag{2}$$

When the wheel looses contact (point "1") the primary suspension spring (of stiffness k) is released. The force acting on the spring accelerates the wheel downwards, while the car body due to its larger inertia ($M \gg m$) is unable to "follow" this movement (this is exactly the role of the primary suspension). So, in the vertical direction (z), the wheel will follow an oscillatory movement:

$$z = \frac{(M+m)g}{k}[1 - \cos(\omega t)] \tag{3}$$

where

$$\omega = \sqrt{k/m} \tag{4}$$

Eventually, the wheel impacts the ramp (see section C–C) at point "2" (see section B–B) with a vertical impact velocity V_z.

The latter (V_z) depends on the geometry of the ramp (inclination), the properties of the metro car (m, M, and k), and the horizontal train velocity V_y. Naturally, V_z will increase with increasing the size, δ, of the gap. δ

depends on the geometry of the crossing and the degree of wear. If the geometry of both the running surface and the wheel was perfect, δ would tend to vanish and wheel passage over the crossing would be a more-or-less smooth transition. However, when the geometry is not perfect, δ becomes larger and wheel passage is dominated by the impact on the ramp. Since the wear increases with time, δ will also be time dependent. A simplified lumped mass model was developed to estimate δ and V_z [6]. Assuming $V_y \approx 22$ m/s (80 km/h, the typical train passage speed), $m \approx 0.75$ t, $M \approx 6.25$ t, and $k \approx 2400$ kN/m (typical values for the SIEMENS vehicles of Attiko Metro), $\delta = 4$–9 mm and $V_z = 0.8$–1.1 m/s (depending on the assumed wear).

10. Dynamic wheel impact analysis

The estimated vertical impact speed of the wheel V_z is utilised to analyse the dynamic response of the system. The sole input to the system is the impacting wheel mass of 0.75 t that reaches the ramp with $V_z = 0.8$–1.1 m/s (point 2, in Fig. 13). Thus, the loading onto the crossover is an impact velocity and not a contact force, allowing the system to dynamically respond naturally. The analysis performed herein is *non-linear transient dynamic*. Micro-cellular pad, rubber boot, sleeper, and concrete sub-base are connected with each other through special interfaces with tension cut-off: they can separate one from the other and de-bond. Therefore, only net compression is transferred from the sleeper to the concrete sub-base, improving the degree of realism in modeling compared to the eigen-frequency analysis (where such non-linearities were not accounted for). As for quasi-static and eigen-frequency analyses, the second *FSI* effect (the effect of gaps and imperfections) is investigated through the effective Poisson ratio ν'. We compare the results for $\nu' = 0.49$ (ideal foundation) and 0.30 (defective foundation with gaps and imperfections).

Fig. 17 illustrates the dynamic response of the system with *ideal foundation* ($\nu' = 0.49$) in the form of six snapshots of the deformed mesh along with vertical displacement Δ_z contours. The impact takes place at $t = 3$ ms, forcing the rail to move downwards. At $t = 4$ ms the rail has almost reached its minimum Δ_z of -1.2 mm while the excitation has not yet been "felt" by the guardrail. The latter follows this downward movement with phase difference, and at $t = 6$ ms the guardrail has reached its minimum Δ_z. Then, at $t = 9$ ms the system starts moving upwards.

The time histories of σ_{xx} in the area of base-plate failure (top of the base flange of plate RP20R) and Δ_z of the rail (crossing) are depicted in Fig. 19a. Clearly, the σ_{xx} time history does not match the measurements

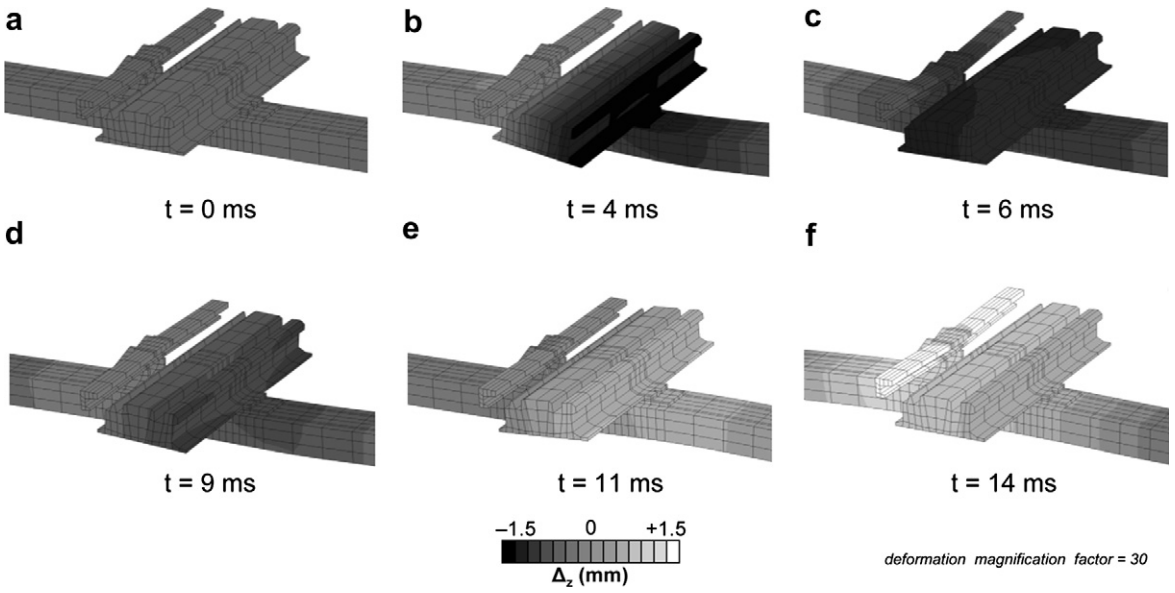

Fig. 17. Dynamic wheel impact analysis – ideal foundation ($\nu' = 0.49$): snapshots of finite element deformed mesh along with contours of vertical displacement Δ_z for $t = 0$ ms, 4 ms, 6 ms, 9 ms, 11 ms, and 14 ms.

(Figs. 8 and 19b). There is only one positive stress peak of $\sigma_{xx} \approx 100$ MPa, not followed by a negative one. In addition, the minimum Δ_z does not exceed 1.2 mm (instead of the measured 3 mm). We utilise the time history of Δ_z to derive the dominant response frequency of the system. Observe that the first displacement pulse takes about 7.5 ms, while the second one (upward displacement) is of little longer duration: 8.5 ms. If we approximate this two-pulse sequence with an equivalent one cycle sinus (a reasonable approximation), then the whole sinusoidal pulse would have a period of 16 ms, indicating a computed dominant natural frequency $f_1 \approx 62$ Hz. This reduction of f_1 (compared to the 91 Hz of the eigen-frequency analysis) is solely attributable to the effect of separation and uplifting. In conclusion, the computed dominant natural frequency of the system, under the assumption of an ideal foundation, is in good agreement with the measured dominant mode (≈54 Hz) of the brand-new crossover X16 (Fig. 10), but the computed σ_{xx} time histories are in disparity with the measured response of the older crossover X20.

The dynamic response of the system with *defective foundation* ($v' = 0.30$) is depicted in Fig. 18, in the form of snapshots of deformed mesh with Δ_z contours. As with ideal foundation (Fig. 17), the rail moves downwards first ($t = 4$ ms) with the guardrail following with a time lag. However, with a defective foundation the downward displacement of the rail reaches $\Delta_z \approx 3$ mm instead of 1.2 mm. In addition, the downward motion of the guardrail is delayed even more ($t = 6$ ms). Then, when the guardrail finally moves down ($t = 10$ ms), their phase difference is so large that it practically ''crashes'' the base flange of the support plate between rail and guardrail (i.e. the area of fatigue failure). The time history of σ_{xx} in the area of failure (Fig. 19b) confirms the increased levels of base-plate distress. Having assumed a defective foundation with gaps and imperfections, led to σ_{xx} that is in good agreement with the measurements. The first positive stress peak of 92 MPa is followed by a negative of −162 MPa, and a third positive peak of 108 MPa. The increased flexibility of the defective foundation seems to have a double detrimental effect: (a) it causes excessive bending of the sleepers leading to larger imposed curvature on the base-plates, and (b) it increases the phase difference between rail and guardrail leading to larger differential displacements. Observe that the second (negative) stress peak takes place when the guardrail is moving downwards relative to the rail. As shown in Fig. 19b the maximum displacement is also in good agreement with the measured reality: 2.8 mm versus 3 mm. Following the previous arguments, from the time history of the vertical displacement we can compute the dominant response frequency of the system. Since the first displacement pulse takes about 15 ms and the second 13 ms, the system responds with a natural frequency $f_1 \approx 35$ Hz, matching closely the measured natural frequency for the case of the older crossover X20 (Fig. 10).

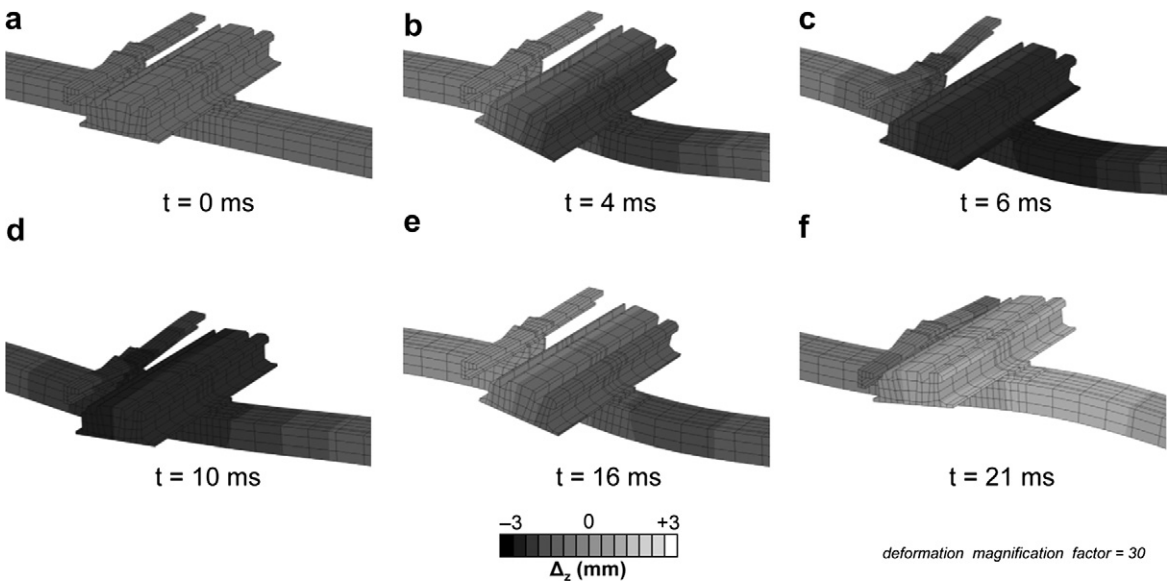

Fig. 18. Dynamic wheel impact analysis – defective foundation with gaps ($v' = 0.30$): snapshots of finite element deformed mesh along with contours of vertical displacement Δ_z for $t = 0$ ms, 4 ms, 6 ms, 10 ms, 16 ms, and 21 ms.

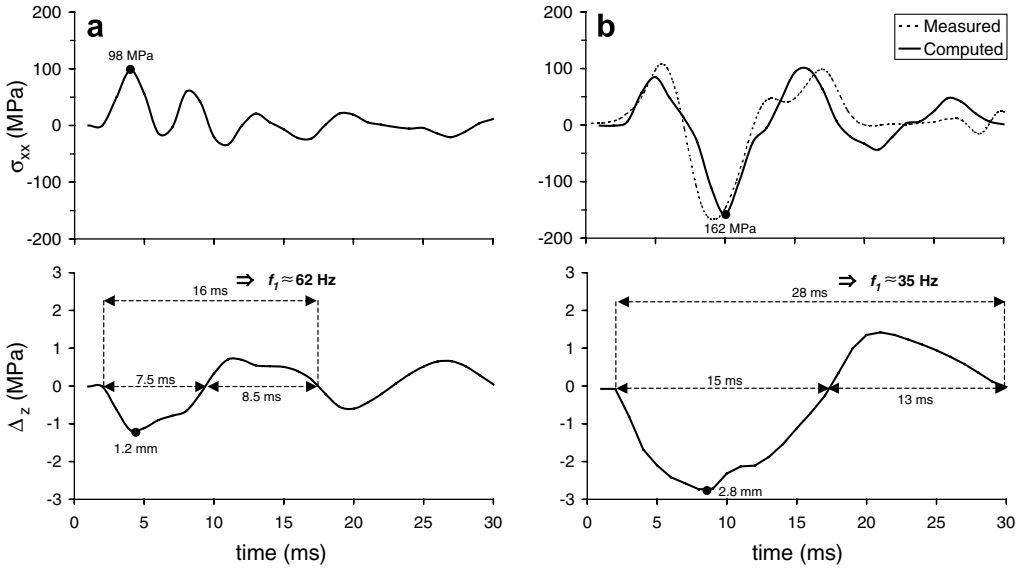

Fig. 19. Dynamic wheel impact analysis – longitudinal stress σ_{xx} (top of plate RP20R) and vertical sleeper displacement Δ_z: (a) ideal foundation; (b) defective foundation with gaps. Only in the second case does the computed stress in the area of failure compare well with the measurements.

11. Conclusions

The main conclusions of our study are:

(1) The role of *foundation–structure interaction* (*FSI*) has been proved to be double and detrimental for the behaviour of the system: (i) the initial defective curved shape of the sleepers induces large bending pre-stress on the base-plates, and (ii) the defective gap-dominated foundation increases the flexibility of the system leading to excessive sleeper bending, and thus to increased distress of the base-plates.

(2) Both of these *FSI* effects are responsible for the observed premature fatigue failure. The initial defective curved shape of the sleepers would not be enough (by itself) to cause failure: excessive vibration due to defective foundation is also required. Conversely, excessive vibration could not be solely responsible: damage would not have occurred if it were not for the accidental initial curvature of the sleepers.

(3) The installation procedure of the sleeper–micro-cellular pad–rubber boot assembly is of critical importance for the reliability and durability of a crossover. Given that this assembly is used as the casing for the concrete sub-base, the quality of the foundation relies on the fastening procedure. With improper installation small gaps and foundation imperfections may be generated.

(4) The more unconfined the micro-cellular pad is (due to gaps), the more it can expand, and consequently the more flexible the system becomes. The decreased stiffness of the foundation results in excessive bending of the sleepers, producing larger stresses at the base-plates.

(5) With defective foundation, besides the increase in maximum stress, the number of stress peaks per wheel passage is also increased. While with an ideal foundation only one peak per wheel is observed, with a defective foundation at least three peaks occur – clearly detrimental for fatigue failure.

(6) Only with a comprehensive model that takes account of foundation deficiencies (i.e. gaps) could we reproduce the measured response. Then, the time history of stress at the location of fatigue failure, the maximum displacement, and the dominant frequency of the system are all in accord with the measurements.

12. Solution to the problem

Having identified the causes of failure, six possible corrective measures were proposed and tentatively tested through FE modeling [6]. The results indicated that the two most effective of them were: (i) the separation of the base-plate from the guardrail support and (ii) the installation of additional supports between the sleepers. The latter, despite its efficiency, was deemed to be unconventional and difficult to implement.

Therefore, SPIE S.A. proceeded in manufacturing a new design in which the guardrail support is separated from the base-plates. The new plates were initially installed on crossover X11, and instrumented to measure stresses during both installation and train passage. The measurements [10] did not show significant stressing neither during installation, nor during train passage. A new parametric FE study was conducted to further verify the effectiveness of the solution. The new study gave emphasis on the pre-stressing of the fixing bolts and the properties of the elastic washers (of Vossloh Fe6 type). It was concluded that the new design is fail-safe provided that over-screwing of the bolts is avoided. It was recommended that the bolt pre-stress did not exceed 15 kN.

In addition, resin was injected between the sleeper and the micro-cellular pad to fill possible foundation gaps. To verify the effectiveness of the method new displacement measurements were undertaken on crossover X20 [11]. The maximum vertical displacement was reduced to $\sim$2 mm (compared to $\sim$3 mm), indicating an increase of the stiffness of the system.

Acknowledgements

We would like to thank the former General Director of Attiko Metro S.A. Mr. Fady Basili for funding the presented work and kindly allowing its publishing. We have benefited greatly from discussions with Monsieur Carl Felix whose help and encouragement were valuable.

References

[1] Von Lange H. Advanced technology turnouts for Class I, short line and mixed freight/passenger rail. A.R.E.A. – Turnout and Special Trackwork Symposium, Chicago, IL, 1996.
[2] Esveld C. Modern Railway Track. second ed. MRT Productions; 2001, ISBN 90-800324-3-3.
[3] TRCpro. Report on force and strain measurements performed on request of Spie for Attiko Metro, Athens, Technical Report to Attiko Metro, Athens, 2001.
[4] TRCpro. Report on stress measurements in guardrail supports performed at Attiko Metro, Athens, Technical Report to Attiko Metro, Athens, 2001.
[5] Seram/Laeis-Weichenbau. Analysis of the failure modes of the Athens Metro turnouts. Technical Report to Attiko Metro, Athens, 2002.
[6] Gazetas G, Anastasopoulos, I. Turnout crossings of the Athens Metro: investigation on the causes of failure of base-plate assemblies through 3-D finite element modeling. Technical Report to Attiko Metro, Athens, 2002.
[7] Attiko Metro SA. Study, construction, operation, running and development of the electrical railways network of Attica Region. http://www.ametro.gr.
[8] Dubbel H, Beitz W, Küttner KH, Davies BJ, editors. Handbook of mechanical engineering. London: Springer-Verlag; 1994.
[9] ABAQUS, Hibbitt, Karlsson, & Sorensen.
[10] Railtech. Stress measurements on moulded parts, Line 2, Crossover 11, Athens Metro, Technical Report to Attiko Metro, Athens, 2003.
[11] Railtech. Displacement measurements, Crossover No. 20, Line 3, Technical Report to Attiko Metro, Athens, 2003.